Lithos 175–176 (2013) 244–254

Contents lists available at SciVerse ScienceDirect

Lithos

journal homepage: www.elsevier.com/locate/lithos

Zircon U–Pb age, geochemical, and Sr–Nd–Hf isotopic constraints on the origin of mafic dykes in the Shaanxi Province, North China Craton, China

Shen Liu [a,*], Caixia Feng [a], Bor-ming Jahn [b], Ruizhong Hu [c], Shan Gao [d], Ian M. Coulson [e], Guangying Feng [f], Shaocong Lai [a], Chaogui Yang [c], Yuhong Yang [c]

[a] State Key Laboratory of Continental Dynamics and Department of Geology, Northwest University, Xi' an 710069, China
[b] Department of Geosciences, National Taiwan University, Taipei, Taiwan
[c] State Key Laboratory of Ore Deposit Geochemistry, Institute of Geochemistry, Chinese Academy of Sciences, Guiyang 550002, China
[d] State Key Laboratory of Geological Processes and Mineral Resources, China University of Geosciences, Wuhan 430074, China
[e] Solid Earth Studies Laboratory, Department of Geology, University of Regina, Regina, Saskatchewan S4S 0A2, Canada
[f] Institute of Geology, Chinese Academy of Geological Sciences, Beijing 100037, China

ARTICLE INFO

Article history:
Received 25 February 2013
Accepted 24 April 2013
Available online 4 May 2013

Keywords:
Palaeozoic
Mafic dykes
Petrogenesis
Shaanxi Province
NCC

ABSTRACT

Mafic dolerite dykes form a series of swarms that are widespread across the North China Craton (NCC). We present U–Pb zircon ages, geochemical data, and Sr–Nd–Hf isotopic data for representative samples of the Shaanxi dolerite dykes in the southern NCC. Laser ablation inductively coupled plasma mass spectrometry (LA-ICP-MS) U–Pb zircon analyses for three samples yield ages ranging from 448.1 ± 1.2 to 489.6 ± 0.9 Ma (i.e., Cambro-Ordovician). The dolerites are characterised by a wide range of rock compositions. They display enrichments in light rare earth element (LREEs) and large ion lithophile element (LILE) (i.e., Ba, U, K and Pb), as well as depletion in high field strength (HFSE) (Nb, Ta, Hf and Ti). The mafic dykes have relatively uniform $(^{87}Sr/^{86}Sr)_i$ ranging from 0.7049 to 0.7076, $(^{176}Hf/^{177}Hf)_i$ from 0.282187 to 0.282236, low ε_{Nd} (t) values, from −4.1 to −4.9, ε_{Hf} (t) values of between −7.9 and −9.8, for zircon, and high hafnium model ages (T_{DM1} = 1366–1535 Ma, T_{DM2} = 1924–2081 Ma). These results suggest that the dykes are derived by partial melting of an enriched, lithospheric mantle source. The magmas underwent fractionation of olivine, pyroxene, plagioclase, and Ti-bearing phases (rutile, ilmenite, titanite), along with crustal contamination. The formation of the Shaanxi Province, NCC mafic dykes can be attributed to the collision between the NCC and south Qinling Block. Specifically, these magmas formed as a result of crustal thinning in response to extension that followed this collision.

1. Introduction

The NCC is composed of three Archaean tectonic units: an Eastern Continent (EC, >2500 Ma), a Western Continent (WC, >2500 Ma), and a Middle Continent (Kusky and Li, 2003; Zhao et al., 2002), and many provinces (e.g., Jilin, Liaoning, Beijing, Inner Mongolia, Hebei, Shanxi, Shandong and Shaanxi,) are located within this ancient cratonic part of China (Fig. 1a). Swarms of more than six hundred mafic dykes (that include dolerite, dolerite-porphyry and lamprophyre) are widespread in the NCC, commonly occurring as NE–NW–WE-trending swarms (Liu et al., 2008a,b, 2009, 2012a,b, 2013). It is generally accepted that these mafic dykes formed as a result of considerable extension of the continental lithosphere (Hall, 1982; Hall and Fahrig, 1987; Tarney and Weaver, 1987; Zhao and McCulloch, 1993). Therefore, studies of the NCC mafic dyke swarms can provide critical insights in our understanding of the generation of extensive mafic magmatism, and also valuable information concerning the lithospheric evolution (extensional process, mantle source, and temporal and spatial evolution) relating to the breakup of the NCC (e.g., Liu, 2004; Liu et al., 2006, 2008a,b, 2009, 2012a,b, 2013), as well as to mineralization present across the NCC.

Although there is some published work on the NCC mafic dykes these studies have focused mainly on the Mesozoic (e.g., Liu, 2004; Liu et al., 2006, 2008a,b, 2009, 2012b, 2013, Yang et al., 2004; Zhang and Sun, 2002) and Precambrian (e.g., Hou et al., 2006, 2008; John et al., 2010; Li et al., 2010; Liu et al., 2012a; Peng, 2010; Peng et al., 2005, 2007, 2008, 2010, 2011a,b) NCC mafic dyke swarms. However, little is known about Paleozoic mafic dykes that are also present. Furthermore, it is generally accepted that significant lithospheric extension occurred during the early Paleozoic in the southern Shaanxi Province; however, the extent of this extension and its timing are still unclear. There is also considerable controversy relating to the timing (Paleozoic or Mesozoic) of collision between the NCC and Yangtze Block. Consequently, the investigation of Palaeozoic crustal

* Corresponding author. Tel./fax: +86 29 88300226.
E-mail addresses: liushen@vip.gyig.ac.cn, liushen@nwu.edu.cn (S. Liu).

0024-4937
http://dx.doi.org/10.1016/j.lithos.2013.04.020

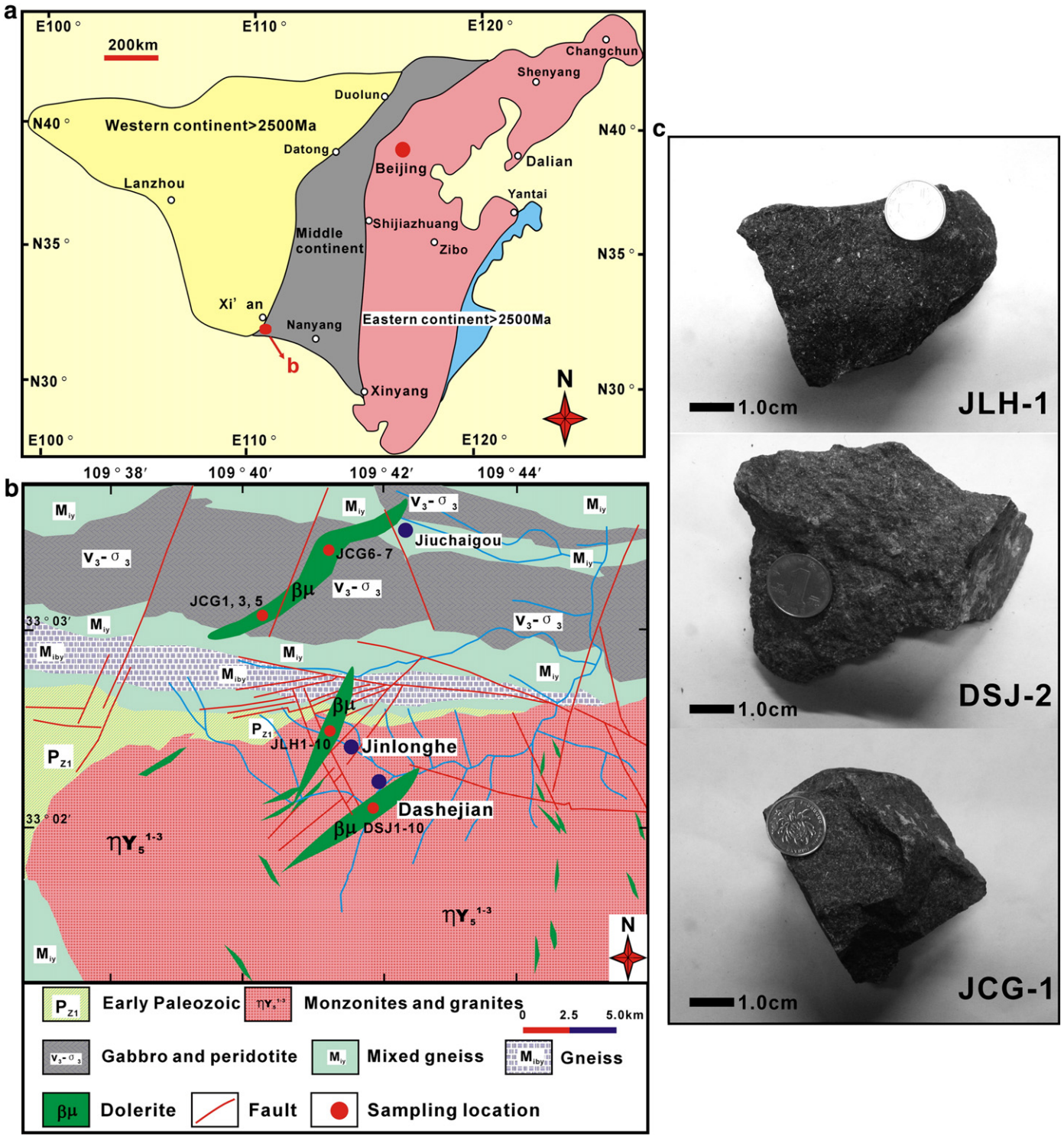

Fig. 1. a. Simplified tectonic map of the NCC, China. b. Inset geological map of the study area as well as the distributions of the mafic dykes, and dyke samples collected for this study. Modified after RGSPS (1982).

extension and related mafic magmatism, through investigation of NCC mafic dyke swarms can provide significant information on a wide range of geological issues.

In this paper we present new laser ablation inductively coupled plasma mass spectrometry (LA-ICP-MS) zircon U–Pb ages, petrography, major, trace element and Sr–Nd–Hf isotopic data for NCC mafic dykes in the Shaanxi region. In doing so we will: (1) constrain the emplacement age(s) of the mafic dykes; (2) determine their petrogenesis; and (3) understand the evolution of the lithospheric mantle beneath the southern NCC.

2. Geological setting and petrography

The NCC comprises two Archaean blocks, an eastern and a western block, that are separated by a 1.8 Ga N–S trending Proterozoic orogenic belt (Middle continent) (Zhao et al., 2001) (Fig. 1a). Two geological

sutures occur in the southern Shaanxi Province, i.e., the Mian-Lue suture and Shang-Dan suture. The more southerly, Mian-Lue suture mainly comprises an ophiolitic mélange, ancient gneiss, granite, mafic volcanic rocks, and mafic dykes, whereas for the northerly Shang-Dan suture, rock types include ophiolite, volcanic rocks, dolomite, and cherts (Shaanxi Province Bureau of Geology and Mineral Resources, 1989).

The mafic dykes are widespread in the Shaanxi Province and study area is situated in the southern section of the Province, southern NCC, near to the Shang-Dan suture (Fig. 1). The country rocks in the area include predominantly, monzonite and granite, gabbro and peridotite, and gneiss, and, although the mafic dykes intrude all of these lithologies, they principally occur within monzonite–granite and gabbro-peridotite (Fig. 1b). Individual mafic dykes are vertical and NE–NW–NS-trending (Fig. 1c); they are commonly 20 m–1.2 km wide and 0.6–12.5 km in length (Fig. 1b). Representative photomicrographs of the mafic dykes in the vicinities of Jiuchaigou, Jinlonghe and Dashejian are provided in Fig. 2. The mafic dyke outcrop as linear features, and the dyke rocks are all dolerite with a typical doleritic texture.

The dykes are massive, locally vesicular, and structure, fine to medium granularity, and dark-grey or grey-green in colour. In addition, the dykes mainly contain sub- to anhedral clinopyroxene (30–50%), elongate to columnar plagioclase (30–45%), and minor olivine, biotite, quartz, apatite, magnetite and ilmenite (<12%). Generally, the clinopyroxene is altered to a mixture of chlorite, amphibole and carbonate minerals, whereas plagioclase locally is replaced by albite, epidote and kaolinite. Rarely, small and altered granite xenoliths occur within the mafic dykes. Dolerite dykes from Jiuchaigou are vertical in outcrop, trend NW, and are typically 6.0–30 m wide and ~350 m long. These grey-green coloured dykes chiefly comprise 30–35% medium-grained phenocrysts of clinopyroxene (2–4 mm) and lath-shaped plagioclase (2–3 mm), within a 65–70% groundmass of clinopyroxene, plagioclase and minor magnetite. In contrast, dolerite from Jinlonghe and Dashejian are also vertical, trend NW–NE, are 1.5–4.0 m wide, and 40–150 m long, and comprise 25–40% medium-coarse grained phenocrysts of clinopyroxene (2–4 mm) and plagioclase (2–3 mm), in a 60–75% matrix of clinopyroxene, plagioclase, minor magnetite and chlorite.

3. Analytical procedures

3.1. U–Pb dating by LA-ICP-MS methods

Zircon was separated from three samples (JLH-1, DSJ-1, and JCG-2) using conventional heavy liquid and magnetic techniques at the Langfang Regional Geological Survey, Hebei Province, China.

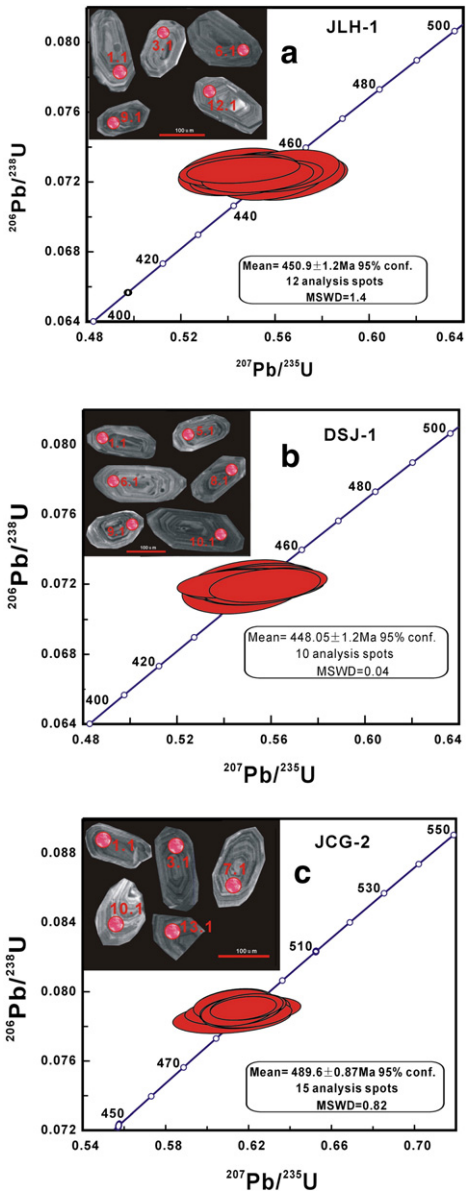

Fig. 3. LA-ICP-MS zircon U–Pb concordia diagrams, and inset CL images of analysed zircon grains, for the investigated mafic dykes from the NCC, China.

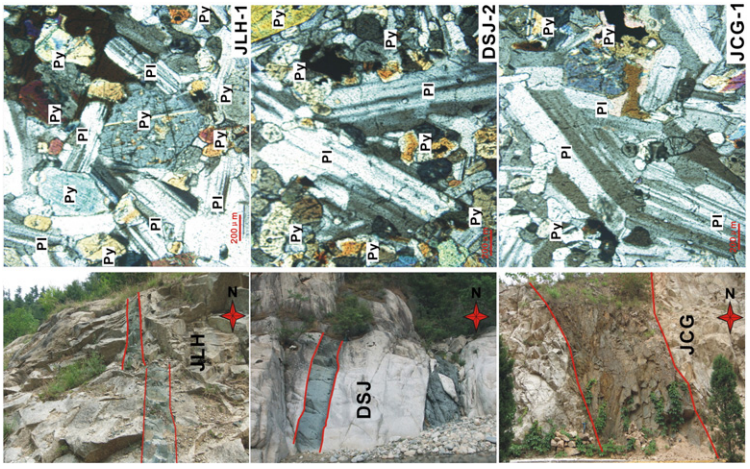

Fig. 2. Representative photomicrographs showing the petrographic features of the mafic dykes from the NCC, China. The samples all display doleritic textures and hence are termed dolerite dykes. Key: Py — pyroxene; Pl — Plagioclase.

Table 2
Major element oxides (wt.%) for the mafic dykes in NCC. LOI, loss on ignition. $Mg^{\#} = 100 * Mg/(Mg + Fe)$ atomic ratio. RV, recommended values; MV, measured values. The values for GSR-1 and GSR-3 are from Wang et al. (2003).

Sample	Rock type	SiO_2	Al_2O_3	Fe_2O_3	MgO	CaO	Na_2O	K_2O	MnO	P_2O_5	TiO_2	LOI	Total	Mg#
JLH-1	Dolerite	55.65	15.52	7.41	4.93	5.37	3.66	2.61	0.10	0.52	1.07	2.63	99.47	57
JLH-3	Dolerite	54.84	15.82	7.45	4.84	5.65	3.61	2.72	0.10	0.53	1.09	2.33	98.98	56
JLH-6	Dolerite	54.74	15.96	7.45	4.53	6.59	3.79	2.13	0.10	0.52	1.06	2.45	99.32	55
JLH-7	Dolerite	54.79	15.86	7.24	4.58	6.20	3.82	2.44	0.10	0.51	1.06	2.81	99.41	56
JLH-8	Dolerite	55.63	15.53	7.20	4.52	6.24	3.80	1.86	0.10	0.52	1.05	2.92	99.37	55
JLH-10	Dolerite	54.82	15.87	7.55	4.95	5.37	3.40	3.11	0.10	0.53	1.08	2.65	99.43	56
DSJ-1	Dolerite	51.45	12.72	9.27	9.48	6.83	2.09	3.77	0.12	0.64	1.27	1.87	99.52	67
DSJ-2	Dolerite	51.51	12.63	9.19	10.41	6.65	2.05	3.75	0.12	0.67	1.25	1.57	99.81	69
DSJ-4	Dolerite	51.56	12.45	9.03	8.74	6.59	2.09	3.73	0.13	0.65	1.22	3.16	99.35	66
DSJ-5	Dolerite	50.79	12.78	11.20	9.68	6.01	2.17	3.69	0.12	0.63	1.25	1.83	100.15	63
DSJ-6	Dolerite	50.74	12.59	10.76	10.09	5.99	1.99	3.55	0.12	0.65	1.29	2.16	99.94	65
DSJ-8	Dolerite	50.33	12.62	8.98	10.36	6.91	2.11	3.56	0.12	0.66	1.22	2.69	99.56	70
DSJ-9	Dolerite	50.60	12.46	8.88	10.26	6.73	2.00	3.58	0.12	0.66	1.20	3.15	99.64	70
JCG-1	Dolerite	53.93	18.08	8.44	2.85	6.88	4.10	0.90	0.22	0.35	0.67	2.93	99.35	40
JCG-3	Dolerite	53.27	18.22	8.63	3.83	6.91	4.26	0.85	0.21	0.32	0.64	2.34	99.46	47
JCG-5	Dolerite	54.09	18.29	7.97	2.96	6.22	4.36	0.85	0.17	0.37	0.58	3.43	99.28	42
JCG-6	Dolerite	54.85	18.63	7.86	3.15	6.34	4.44	0.97	0.18	0.31	0.56	2.15	99.44	44
JCG-7	Dolerite	54.02	18.35	7.94	2.85	6.25	4.46	0.84	0.17	0.32	0.57	3.45	99.21	42
GSR-3	RV*	44.64	13.83	13.4	7.77	8.81	3.38	2.32	0.17	0.95	2.37	2.24	99.88	
GSR-3	MV*	44.75	14.14	13.35	7.74	8.82	3.18	2.3	0.16	0.97	2.36	2.12	99.89	
GSR-1	RV*	72.83	13.4	2.14	0.42	1.55	3.13	5.01	0.06	0.09	0.29	0.7	99.62	
GSR-1	MV*	72.65	13.52	2.18	0.46	1.56	3.15	5.03	0.06	0.11	0.29	0.69	99.70	

Zircon separates were examined under transmitted and reflected light, as well as by cathodoluminescence petrography (CL) at the State Key Laboratory of Continental Dynamics, Northwest University, China to observe their external and internal structures. Laser-ablation techniques were employed for zircon age determinations (Table 1 — Supplemental table; Fig. 3) using an Agilent 7500a ICP-MS instrument equipped with a 193 nm excimer laser at the State Key Laboratory of Geological Processes and Mineral Resources, China University of Geoscience, Wuhan, China. Zircon # 91500 was used as a standard, and NIST 610 was used to optimise the results. A spot diameter of 24 μm was used. Prior to LA-ICP-MS zircon U–Pb dating, the surfaces of the grain mounts were washed in dilute HNO_3 and pure alcohol to remove any potential lead contamination. Details of the analytical methodology have been described in the studies of Yuan et al. (2004) and Liu et al. (2010). Corrections for common Pb were performed following Andersen (2002). Data were processed using the GLITTER and ISOPLOT programs (Ludwig, 2003) (Table 1 — Supplemental table; Fig. 3). Errors for individual analyses by LA-ICP-MS were quoted at the 95% (1σ) confidence level.

3.2. Major elemental and trace elemental analyses

Eighteen samples were analysed for major and trace element and Sr–Nd isotopes. Whole-rock samples were trimmed to remove altered surfaces, cleaned with de-ionised water, and then crushed and powdered using an agate mill. Major elements were determined using a PANalytical Axios-advance (Axios PW4400) X-ray fluorescence spectrometer (XRF) at the State Key Laboratory of Ore Deposit Geochemistry, Institute of Geochemistry, Chinese Academy of Sciences. Fused glass discs were utilised and the analytical precision was better than 5%, as determined based on the Chinese National standards: GSR-1 and GSR-3 (Table 2). Loss on ignition (LOI) was obtained using 1 g of powder heated to 900 °C for 2 h. Trace elements were analysed by plasma optical emission mass-spectrometry (MS) and ICP-MS at the National Research Center of Geo-analysis, Chinese Academy of Geosciences. The discrepancy among triplicates was less than 5% for all elements. Analysis results of the international standards OU-6 and GBPG-1 were in agreement with the recommended values (Table 3).

3.3. Sr–Nd isotopic analyses

For the analysis of Rb–Sr and Sm–Nd isotopes, sample powders were spiked with mixed isotope tracers, dissolved in Teflon capsules with $HF + HNO_3$ acids, and separated by conventional cation-exchange techniques. Isotopic measurements were performed using a Finnigan Triton Ti thermal ionisation mass spectrometer at the State Key Laboratory of Geological Processes and Mineral Resources, China University of Geosciences, Wuhan, China. Procedural blanks were <200 pg for Sm and Nd, as well as <500 pg for Rb and Sr. Mass fractionation corrections for Sr and Nd isotopic ratios were based on $^{86}Sr/^{88}Sr = 0.1194$ and $^{146}Nd/^{144}Nd = 0.7219$, respectively. Analyses of standards yielded the following results: NBS987 gave $^{87}Sr/^{86}Sr = 0.710246 \pm 16$ (2σ) and La Jolla gave $^{143}Nd/^{144}Nd = 0.511863 \pm 8$ (2σ). The analytical results for Sr–Nd isotopes are presented in Table 4.

3.4. In situ zircon Hf isotopic analysis

In situ, zircon Hf isotopic analyses were conducted using a Neptune multiple collector (MC)-ICP-MS, equipped with a 193 nm laser, at the Institute of Geology and Geophysics, Chinese Academy of Sciences in Beijing, China. During the analysis, a laser repetition rate of 10 Hz at 100 mJ was used, as were spot sizes of 32 and 63 μm. Details of the analytical technique are described in Wu et al. (2006). During the analysis, the $^{176}Hf/^{177}Hf$ and $^{176}Lu/^{177}Hf$ ratios of the standard zircon (91500) were 0.282300 ± 15 ($2\sigma n$, $n = 24$) and 0.00030, similar to the commonly accepted $^{176}Hf/^{177}Hf$ ratio of 0.282302 ± 8 and 0.282306 ± 8 (2σ) measured using the solution method (Goolaerts et al., 2004). The analytical results are listed in Table 5 (Supplemental table).

4. Results

4.1. Zircon U–Pb ages

Euhedral zircon grains in samples JLH-1, DSJ-1, and JCG-2 are clean and prismatic, with magmatic oscillatory zoning (Fig. 3). A total of 12 grains provided a weighted mean $^{206}Pb/^{238}U$ age of 450.9 ± 1.2 Ma (1σ) (95% confidence interval) for JLH-1; 10 grains have a weighted mean $^{206}Pb/^{238}U$ age of 448.1 ± 1.2 Ma (1σ) (95% confidence interval) for DSJ-1, and 15 grains gave a weighted mean $^{206}Pb/^{238}U$ age of 489.6 ± 0.9 Ma (1σ) (95% confidence interval) for JCG-2 (Table 1 — Supplemental table; Fig. 3a–c). These determinations are the best estimates of the crystallisation ages of the dolerite dykes. There was no inherited zircon characteristics observed.

4.2. Major and trace elements

Geochemical data on the mafic dykes in the study area are presented in Tables 2 and 3. The dolerite samples exhibit a wide range of geochemical compositions, falling into both the alkaline (JLH and DSJ) and calc-alkaline fields (JCG) in terms of the total alkali-silica (TAS) diagram (Fig. 4a); rock types include basaltic andesite, basaltic trachy-andesite, andesite, and trachy-andesite. The JLH and DSJ dyke samples also display an affinity to shoshonitic compositions, whereas JCG samples are again calc-alkaline, in terms of Na_2O vs. K_2O (Fig. 4b). The dykes display regular trends of decreasing TiO_2, Fe_2O_3, and MgO with increasing SiO_2 (Fig. 5b, c, d) and are also characterised by LREE enrichment and HREE depletion, with a wide range in La/Yb ratios and Eu_N/Eu^* (Table 3 and Fig. 6a). On primitive mantle-normalised trace element diagrams, the mafic samples show enrichment in LILEs (i.e., Ba, U, K, and Pb) and depletion in HFSEs (i.e., Nb, Ta, Hf, and Ti) (Fig. 6b).

4.3. Sr–Nd isotopes

Sr–Nd isotopic data have been obtained from (twelve) representative mafic dyke samples (Table 4). The dykes show very different $(^{87}Sr/^{86}Sr)_i$ values ranging from 0.7049 to 0.7076, and relatively little variation in ε_{Nd} (t) values from −4.1 to −4.9. The Sr–Nd isotopic compositions (Fig. 7) are also comparable to those of early Palaeozoic mafic rocks determined previously for the NCC.

4.4. Zircon Hf isotopes

Three samples of zircon dated by U–Pb methods were also analysed for their Lu–Hf isotopes, and the results are presented in Table 5 (Supplemental table). Sixteen spot analyses were obtained for the zircon sample, JLH-1, yielding variable ε_{Hf} (t) values of between −8.6 and −9.0 (Fig. 8a), with two-stage model ages (T_{DM2}) of 1968 to 1997 Ma (Fig. 8d), and giving initial $^{176}Hf/^{177}Hf$ ratios ranging from 0.282236 to 0.282249. Fifteen spot analyses were made for sample DSJ-1. The determined negative ε_{Hf} (t) values for this zircon vary between −7.9 and −8.2 (Fig. 8b), corresponding to T_{DM2} model ages in the range of 1924 to 1944 Ma (Fig. 8e). This sample has an initial $^{176}Hf/^{177}Hf$ ratio that varies between 0.282261 and 0.282271. Fifteen spot analyses were also performed on zircon from sample JCG-2. The determined negative ε_{Hf} (t) values for this dyke vary between −9.4 and −9.9 (Fig. 8c), corresponding to T_{DM2} model ages in the range of 2049 to 2081 Ma (Fig. 8f). This sample has initial $^{176}Hf/^{177}Hf$ ratios that vary between 0.282187 and 0.282200. The zircon Hf isotopic results also suggest an enriched mantle source region for the mafic dykes.

5. Genetic discussion

5.1. Mantle source

The Paleozoic Shanzi Province mafic dykes are characterised by low SiO_2 contents (50.3–55.7 wt.%), suggesting that the mafic dykes were derived from an ultramafic source. This is supported in the high MgO contents (4.5–10.4 wt.%) and $Mg^{\#}$ (55–70) in the mafic dykes from JLH1-10 and DSJ1-9. Crustal rocks can be ruled out as possible sources, as partial melting of any of the crustal rocks (e.g., Hirajima et al., 1990) and lower crustal intermediate granulites (Gao et al., 1998) in the deep crust would produce high-Si, low-Mg liquids (i.e., granitoid liquids; Rapp et al., 2003). The high initial $^{87}Sr/^{86}Sr$ ratios and negative ε_{Nd} (t) and zircons ε_{Hf} (t) values (Tables 4 and 5 — Supplemental tables) for the mafic dykes are consistent with a derivation from an enriched lithospheric mantle source rather than an asthenospheric mantle-source, with a depleted Sr–Nd isotopic composition, such as MORB.

Table 3
Trace element compositions (in ppm) for the mafic dykes from NCC.
The values for GBPG-1 are from Thompson et al (2000), and for OU-6 from Potts and Kane (2005).

Sample	JLH-1	JLH-3	JLH-6	JLH-7	JLH-8	JLH-10	DSJ-1	DSJ-2	DSJ-4	DSJ-5	DSJ-6
V	158	166	175	171	168	168	170	174	178	171	171
Cr	79.3	76.2	73.7	73.4	73.1	74.6	425	449	446	425	441
Ni	36.4	36.2	35.3	36.1	34.5	36.2	377	416	253	356	397
Ga	17.4	18.2	20.9	20.2	19.5	18.3	16.2	16.2	16.7	16.7	16.4
Rb	89.2	89.1	69.3	78.9	61.8	107.0	88.4	85.3	86.3	85.4	86.3
Sr	940	979	1160	1090	1080	947	617	590	715	615	603
Y	15.7	15.8	16.0	15.7	15.6	16.2	27.6	26.6	26.5	27.6	27.6
Zr	147	147	150	146	147	150	379	343	337	373	362
Nb	10.5	10.7	10.6	10.6	10.5	10.7	12.9	12.0	12.3	12.7	12.4
Ba	1410	1440	1000	1290	825	1450	1519	1049	1069	1049	1059
La	29.0	28.1	28.9	27.8	29.6	29.1	32.9	30.0	33.4	32.4	31.4
Ce	57.4	56.8	59.3	56.5	58.9	59.7	71.6	66.4	73.1	70.4	68.1
Pr	7.06	6.75	6.96	7.00	7.06	7.38	9.09	8.50	9.18	8.80	8.64
Nd	27.1	27.1	27.4	27.7	28.0	27.9	38.0	36.6	39.3	36.7	36.8
Sm	5.04	5.30	5.02	4.93	5.05	5.36	8.13	7.95	8.32	8.09	7.97
Eu	1.46	1.44	1.41	1.40	1.46	1.43	2.09	1.97	2.09	2.07	2.01
Gd	3.88	4.18	3.90	3.84 3.90	4.33	7.32	7.14	7.33	6.90	6.73	6.90
Tb	0.62	0.61	0.61	0.58	0.64	0.61	0.99	0.98	1.04	0.99	1.03
Dy	3.01	2.87	2.95	2.99	2.92	3.00	5.50	5.42	5.46	5.39	5.62
Ho	0.62	0.63	0.63	0.61	0.62	0.62	1.01	1.01	0.98	1.00	1.03
Er	1.56	1.56	1.56	1.56	1.55	1.59	2.71	2.63	2.65	2.70	2.72
Tm	0.21	0.20	0.22	0.22	0.21	0.22	0.34	0.34	0.32	0.35	0.37
Yb	1.33	1.37	1.35	1.33	1.28	1.36	2.33	2.22	2.14	2.31	2.35
Lu	0.19	0.19	0.19	0.18	0.19	0.18	0.33	0.32	0.30	0.32	0.33
Hf	3.54	3.64	3.61	3.51	3.56	3.68	10.6	9.56	9.02	10.0	10.4
Ta	0.52	0.54	0.54	0.58	0.53	0.52	0.83	0.77	0.74	0.83	0.80
Pb	8.38	9.79	14.40	12.20	11.60	9.22	16.3	14.4	18.9	15.9	15.5
Th	3.45	3.40	3.50	3.51	3.49	3.64	5.96	5.68	6.34	6.25	5.59
U	0.96	2.64	1.22	4.41	1.10	2.00	1.79	1.73	1.79	1.78	1.71
δEu	1.0	0.9	1.0	1.0	1.0	0.9	0.8	0.8	0.8	0.8	0.8
$(La/Yb)_N$	15.6	14.7	15.4	15.0	16.6	15.3	10.1	9.7	11.2	10.1	9.6

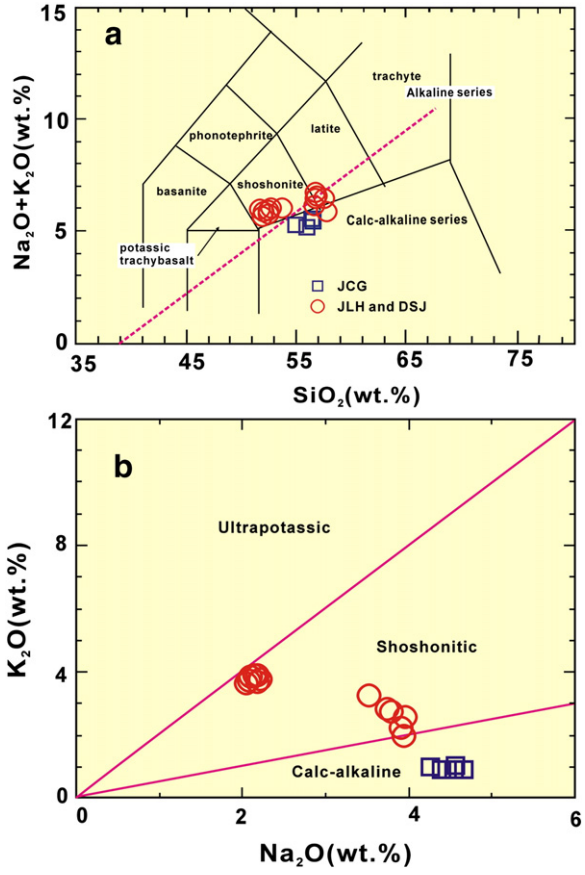

Fig. 4. Classification of the mafic dykes from NCC based upon: (a) TAS diagram. All major elemental data have been recalculated to 100% on a LOI-free basis (after Middlemost, 1994; Le Maitre, 2002). (b) K_2O versus Na_2O diagram. The alkaline association for JLH and DSJ samples is shown to be shoshonitic, whereas JCG samples are calc-alkaline.

5.2. Crustal contamination

Crustal contamination might cause a significant depletion in Nb–Ta and enriched Sr–Nd isotopic signatures in basaltic rocks. The dolerites are characterised by negative Nb–Ta anomalies, high Sr isotopic composition and negative ε_{Nd} (t) (Table 3); this could imply a crustal component in the magma genesis of the mafic dykes. Further support for this is given in their low Nb/U ratios (2.4–11.03) (cf. Nb/U = 9.0–21 for crust, and Nb/U = 47 for primitive mantle), and Ta/La ratios (0.013–0.026) (cf. Ta/La = 0.06 for primitive mantle). Moreover, crustal assimilation would cause a significant variation in Sr–Nd isotopes, and result in a positive correlation between MgO and ε_{Nd} (t) values (−4.1 to −4.9); and features that are also observed in these dolerites (Table 4; Figs. 7 and 9b). There is no correlation between MgO and Sr isotopic rations (Fig. 9a); however this does not rule out crustal contamination, because MgO contents are not solely associated with crustal contamination, but also with fractionation of ferromagnesian phases during magma evolution. In summary, the geochemical and isotopic signatures of the dolerites indicate that crustal contamination occurred.

5.3. Fractional crystallisation

For the studied rocks, JLH1-10 and DSJ19 mafic dyke samples have high $Mg^{\#}$ (55–70) (Table 2), which is inconsistent with significant fractionation. However, the JCG1-7 samples contain lower MgO (< 4.0 wt.%), Cr (<21 ppm) and Ni (<8.0 ppm) (Tables 1 and 2; Fig. 5d), implying that they were derived by fractional crystallisation. Furthermore, SiO_2 shows a negative correlation with TiO_2, Fe_2O_3, and MgO for all rocks (Fig. 5a, c, and d), indicating that the mafic dykes were likely the result of olivine, pyroxene-dominated and Ti-bearing phase (rutile, ilmenite, titanite) fractionation of a more mafic parental magma. Similarly, the separation of plagioclase and Ti-bearing phases could account for the observed

DSJ-8	DSJ-9	JCG-1	JCG-3	JCG-5	JCG-6	JCG-7	OU-6(RV*)	OU-6(MV*)	GBPG-1(RV*)	GBPG-1(MV*)
181	170	161	189	169	143	159	129	131	96.5	103
464	457	13.2	15.1	16.1	20.6	17.1	70.8	73.5	181	187
397	384	5.58	7.67	7.39	6.07	7.50	39.8	42.5	59.6	60.6
16.2	15.9	17.9	16.2	15.3	16.1	14.8	24.3	26.5	18.6	20.9
91.4	87.6	28.1	24.9	20.6	33.4	35.2	120	122	56.2	61.4
596	619	774	822	518	381	286	131	136	364	377
27.0	26.9	28.2	23.1	22.5	23.3	22.0	27.4	26.2	18.0	17.2
354	342	92.5	81.2	76.8	80.5	72.8	174	183	232	224
12.1	12.2	4.69	3.60	3.83	4.35	4.50	14.8	15.3	9.93	8.74
1110	1049	260	297	258	361	376	477	486	908	921
31.5	30.9	21.1	17.1	15.8	16.8	15.3	33.0	33	53.0	51
68.6	66.6	41.8	32.2	31.4	32.7	31.3	74.4	78	103	105
8.79	8.34	5.18	3.92	3.93	4.07	3.84	7.80	8.1	11.5	11.6
37.3	35.9	21.2	16	15.6	17.2	15.8	29.0	30.6	43.3	42.4
7.97	7.86	4.83	3.71	3.72	3.94	3.82	5.92	5.99	6.79	6.63
2.07	2.03	1.62	1.22	1.26	1.33	1.02	1.36	1.35	1.79	1.69
6.95	4.56	3.81	3.66	3.93	3.56	5.27	5.50	4.74	4.47	
0.98	0.95	0.78	0.64	0.64	0.62	0.62	0.85	0.83	0.60	0.59
5.36	5.24	4.56	3.65	3.69	3.74	3.7	4.99	5.06	3.26	3.17
0.99	0.99	1.05	0.89	0.85	0.88	0.85	1.01	1.02	0.69	0.66
2.64	2.58	3.13	2.41	2.36	2.48	2.45	2.98	3.07	2.01	2.02
0.34	0.34	0.46	0.37	0.35	0.37	0.36	0.44	0.45	0.30	0.29
2.24	2.28	3.12	2.38	2.47	2.52	2.51	3.00	3.09	2.03	2.03
0.33	0.31	0.50	0.38	0.38	0.41	0.38	0.45	0.47	0.31	0.31
10.0	9.65	2.37	2.1	1.98	2.01	1.95	4.70	4.86	6.07	5.93
0.80	0.75	0.25	0.21	0.21	0.23	0.20	1.06	1.02	0.40	0.46
15.1	14.1	10.6	9.3	10.2	15.8	11.8	28.2	32.7	14.1	14.5
5.75	5.09	4.23	3.50	3.18	3.27	3.11	11.5	13.9	11.2	11.4
1.73	1.55	1.34	0.92	1.02	1.21	0.77	1.96	2.19	0.90	0.99
0.9	0.8	1.1	1.0	1.0	1.0	0.8				
10.1	9.7	4.9	5.2	4.6	4.8	4.4				

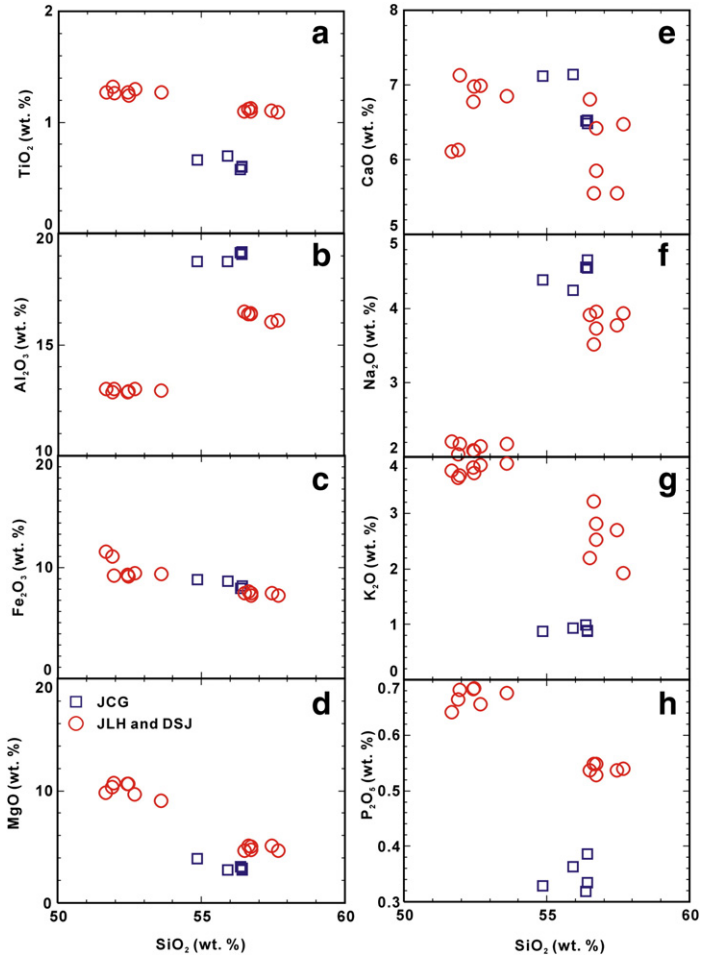

Fig. 5. Selected variation diagrams of major element oxides versus SiO_2 (in wt.%) for the mafic dykes from the NCC, China.

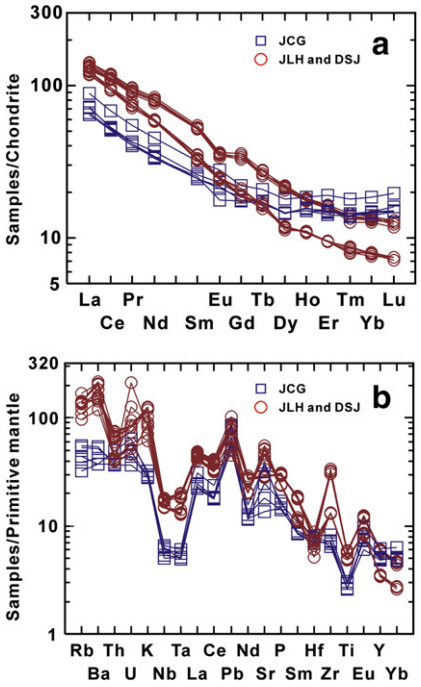

Fig. 6. a) Chondrite-normalised rare earth element (REEs) diagram and b) primitive mantle-normalised incompatible element distribution diagrams for the investigated mafic dykes from the NCC, China.
The normalisation values are from Sun and McDonough (1989).

negative Eu, Nb and Ta anomalies in chondrite-normalised REE patterns and primitive-mantle-normalised trace element patterns (Fig. 6a and b). Additionally, in Eu_N/Eu^* vs. Sr and Ba related plots (online Appendix), the dolerites show a combined vector of K-feldspar and plagioclase fractionation, however, this also indicates that plagioclase fractionation was more important than K-feldspar in controlling Sr and Ba abundances (Table 3).

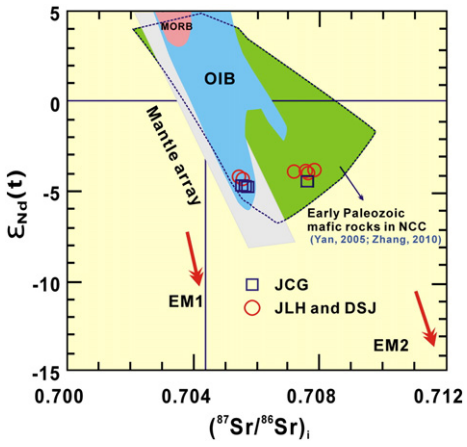

Fig. 7. Initial $^{87}Sr/^{86}Sr$ vs. ε_{Nd} (t) diagram for the studied mafic dykes from the NCC, China. The field for early Palaeozoic mafic rocks from the NCC (after Yan, 2005; Zhang, 2010) is plotted for comparison. The investigated NCC mafic dykes fall within this field, indicating an enriched mantle source.

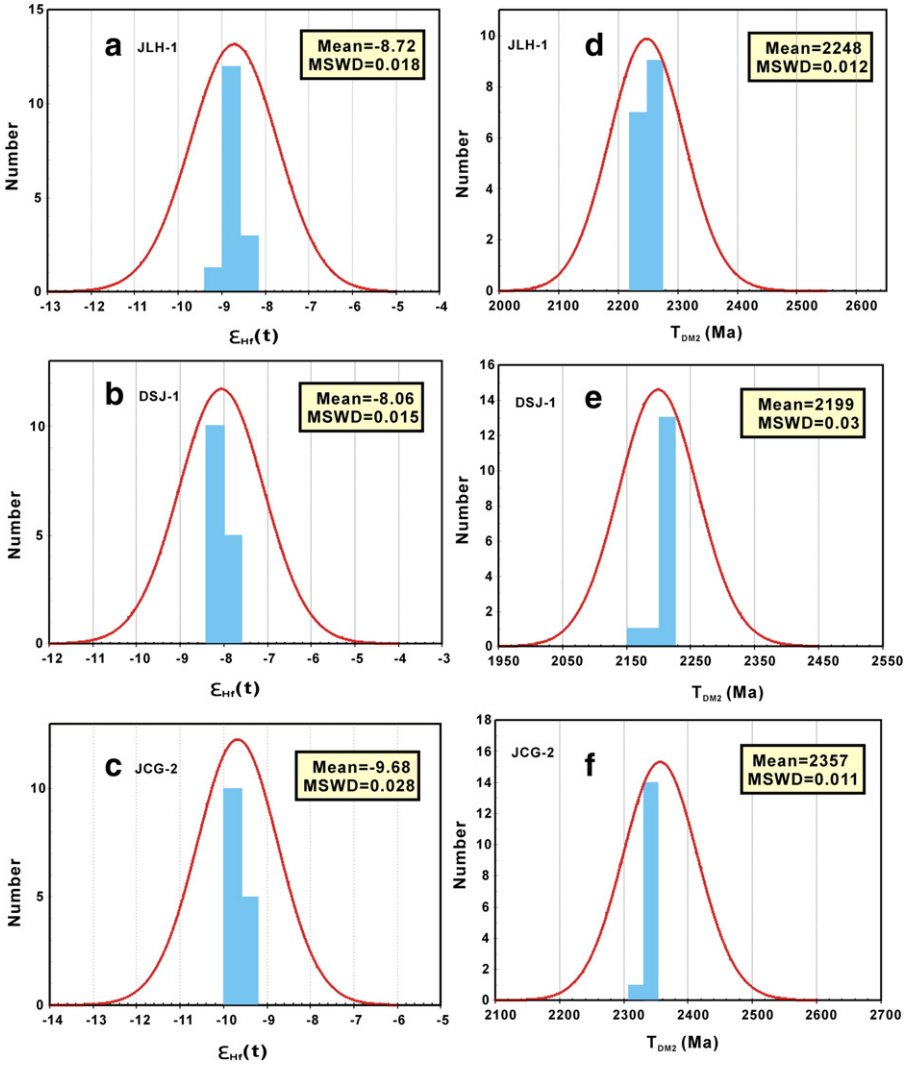

Fig. 8. Histograms of zircon ε_{Hf} (t) values (a to c) and two-stage Hf model ages (d to f) for the mafic dykes in the NCC, China.

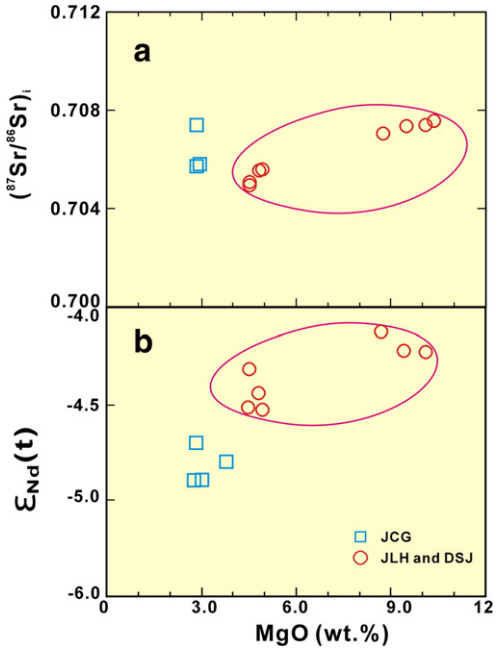

Fig. 9. Plots of: (a) initial $^{87}Sr/^{86}Sr$ ratio and (b) ε_{Nd} (t) value versus MgO for the mafic dykes from the NCC, China.

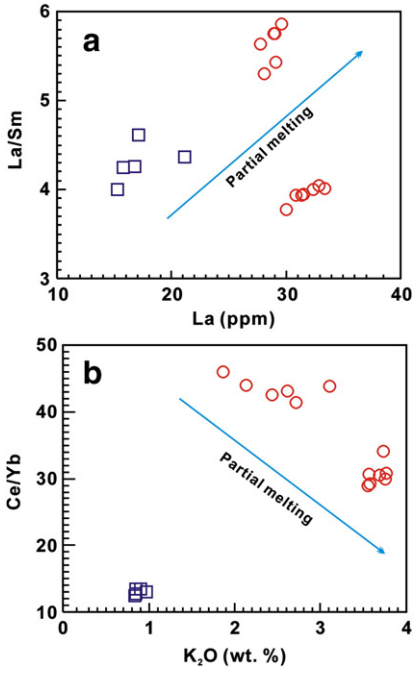

Fig. 10. Plots of (a) La vs. La/Sm and (b) K_2O vs. Ce/Yb for the studied mafic dykes.

5.4. Genetic mechanism and model

The mafic dykes in this study have similar characteristics in terms of geochemistry and isotopes (Sr–Nd–Hf), implying that they have a similar source region. However, they do not result from the same episode of magmatism due to different ages. On plots of La vs. La/Sm and K_2O vs. Ce/Yb related plots (Fig. 10) presented, all samples distribute along the partial melting trend line, indicating that the mafic dykes were derived from partial melting of the enriched mantle.

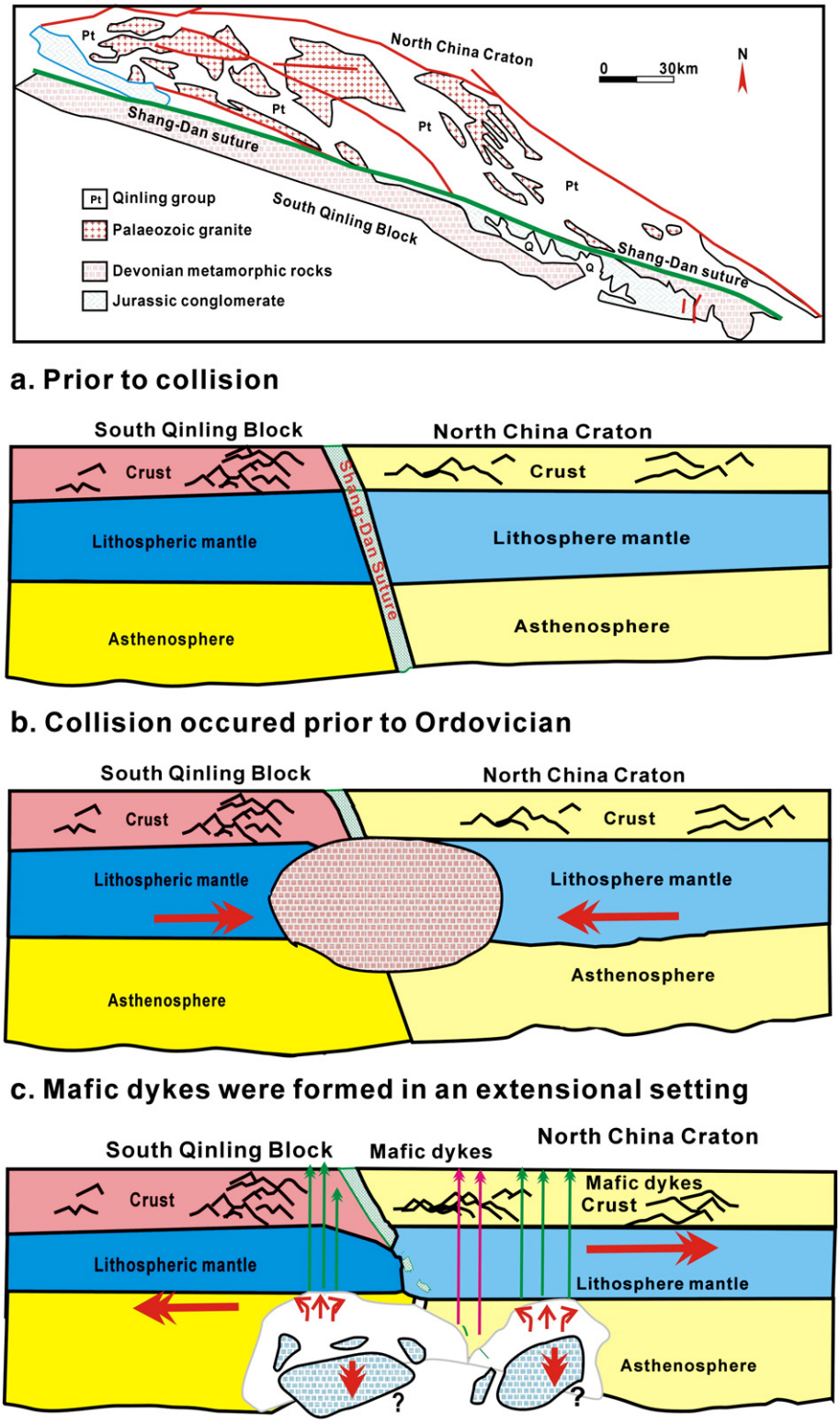

Fig. 11. Schematic models for block collision and the origin of the NCC mafic dykes. (a) Prior to collision between the NCC and the south Qinling blocks. (b) Collision occurred prior to the Ordovician, whereby NCC and the south Qinling Block came together along the Shang-Dan suture, resulting in crustal shortening, deformation and metamorphism within the collisional belt. (c) After collision, the study area underwent extension and thinning, leading to asthenospheric upwelling, local raised geotherms and partial melting of mantle lithosphere. These partial melts are the parental magmas to the NCC, Shaanxi Province mafic dyke swarms.

Based on the above discussion, the mafic dykes in this study are derived through the partial melting of an enriched mantle source. A dynamic model, however, is required to decipher the origin of these mafic dykes. At least two competing mechanisms can be envisaged: (1) the contribution of the subducting Yangtze Block; (2) the action of subducted ancient Pacific Plate (i.e., Izanagi Plate). However, it is generally believed that the final collision between NCC and Yangtze Block occurred during the Triassic (Meng and Zhang, 1999; Zhang et al., 2005), and there was no west-trending subduction of an ancient Pacific Plate towards the NCC before the early Cretaceous (Xu et al., 1993). As the investigated dykes were emplaced during the early Paleozoic, it is unlikely that their petrogenesis relates to either subducting Yangtze lithosphere or the ancient Pacific Plate. An alternative model, therefore, is required to account for how the mafic dykes were formed.

The study area lies to the north of the Shang-Dan suture that separates the NCC and south Qinling Block. During the early Paleozoic (Cambrian), significant collision occurred between the NCC and south Qinling Block (Meng and Zhang, 1999). Following the terminal phase of collision, this boundary underwent extension and gravitational collapse, that resulted in the formation of many extensional basins in this region (e.g., the An'Kang-Ziyang and Wudu-Dibu basins), and also led to alkaline magmatism, and the emplacement of swarms of mafic dyke. We propose, therefore, the following genetic model to account for the presence of the investigated Shaanxi Province mafic dykes: a) prior to collision, the NCC and south Qinling were two independent crustal blocks (Fig. 11a, b) Prior to the Ordovician (>500 Ma), collision between the NCC and south Qiling Block occurred resulting in the formation of the Shang-Dan suture. Crustal shortening and collision resulted in thickening of the lithospheric mantle beneath both the NCC and south Qinling Block. The thickened lithosphere led to deformation and regional metamorphism, at the same time in the zone of collision, supracrustal rocks underwent transformation to produce ophiolite (Fig. 11b, c) Density differences in this mélange resulted in gravitational imbalance, leading to the foundering of denser crustal units into asthenosphere.

Following the terminal stage of collision between the two crustal blocks, relaxation and lithospheric extension occurred (Fig. 11c). Lithospheric extension allowed for buoyant upwelling of hot asthenosphere, which locally raised geothermal gradients, causing partial melting of the lithospheric mantle beneath both the NCC and south Qinling Block. These partial melts represent the parental mafic magmas to the investigated Shaanxi Province dykes.

Foundering of denser crustal units into asthenosphere is supported, moreover, by the voluminous coeval magmatism (Shaanxi Province Bureau of Geology and Mineral Resources, 1989), large-scale mineralization (e.g., Shaanxi Province Bureau of Geology and Mineral Resources, 1989), and the 453 Ma adakitic rocks observed in adjacent areas (e.g., Gujiagou, Nangou and Chenjiagou,), as lithospheric foundering would result in all of these features.

6. Conclusions

Based upon geochronological, geochemical, and Sr–Nd and Hf isotopic studies, the following conclusions have been drawn:

1. U–Pb zircon dating indicates that the studied Shaanxi Province mafic dykes formed between 448.1 ± 1.2 and 489.6 ± 0.9 Ma (i.e., they are late Cambrian–Ordovician).
2. The mafic dykes are derived from an enriched mantle source, with parental magmas originating through the partial melting of the enriched mantle lithosphere beneath both the southern part of the NCC and the south Qinling Block, in response to lithospheric thinning/extension. The parental magmas to the mafic dyke swarms underwent crustal contamination and crystal fractionation during ascent that included the following mineral phases: olivine, pyroxene, plagioclase and Ti-bearing phases (rutile, ilmenite, and titanite).
3. The studied mafic dykes were derived in an extensional setting after the collision between NCC and south Qinling Block.

Supplementary data to this article can be found online at http://dx.doi.org/10.1016/j.lithos.2013.04.020.

Acknowledgements

The present research was supported by the Knowledge Innovation Project (KZCX2-YW-111-03), and the opening project (08LCD08) of State Key Laboratory of Continental Dynamics. The authors gratefully acknowledge Lian Zhou for assistance with the Sr–Nd isotope analyses, Zhaochu Hu for his help with LA-ICP-MS zircon U–Pb dating, and Jinhui Yang for help with the zircon Hf isotope determination. In addition, editor in chief Andrew Kerr and two anonymous reviewers also are thanked for quickly handling this paper.

References

Andersen, T., 2002. Correction of common lead in U–Pb analyses that do not report ^{204}Pb. Chemical Geology 192, 59–79.
Gao, S., Zhang, B.-R., Jin, Z.-M., Kern, H., Luo, T.-C., Zhao, Z.-D., 1998. How mafic is the lower continental crust? Earth and Planetary Science Letters 106, 101–117.
Goolaerts, A., Mattielli, N., de Jong, J., Weis, D., Scoates, J.S., 2004. Hf and Lu isotopic reference values for the zircon standard 91500 by MC–ICP-MS. Chemical Geology 206, 1–9.
Hall, H.C., 1982. The importance and potential of mafic dyke swarms in studies of geodynamic process. Geosciences Canada 9, 145–154.
Hall, H.C., Fahrig, W.F., 1987. Mafic dyke swarms. Geological Association of Canada Special Paper 34, 1–503.
Hirajima, T., Ishiwatari, A., Cong, B., Zhang, R., Banno, S., Nozaka, T., 1990. Coesite from Mengzhong eclogite at Donghai county, northern Jiangsu Province, China. Mineralogy Magazine 54, 579–583.
Hou, G.T., Liu, Y.L., Li, J.H., 2006. Evidence for 1.8 Ga extension of the Eastern Block of the North China Craton from SHRIMP U–Pb dating of mafic dyke swarms in Shandong Province. Journal of Asian Earth Sciences 27, 392–401.
Hou, G.T., Santosh, M., Qian, X.L., Lister, G.S., Li, J.H., 2008. Configuration of the Late Paleoproterozoic supercontinent Columbia: insights from radiating mafic dyke swarms. Gondwana Research 14, 395–409.
John, D.A.P., Zhang, J.S., Huang, B.C., Andrew, P.R., 2010. Palaeomagnetism of Precambrian dyke swarms in the North China Shield: the 1.8 Ga LIP event and crustal consolidation in late Palaeoproterozoic times. Journal of Asian Earth Sciences 41, 504–524.
Kusky, T.M., Li, J.-H., 2003. Palaeoproterozoic tectonic evolution of the North China craton. Journal of Asian Earth Sciences 22, 383–397.
Le Maitre, R.W., 2002. Igneous Rocks: A Classification and Glossary of Terms, 2nd ed. Cambridge University Press, Cambridge 236.
Li, T.S., Zhai, M.G., Peng, P., Chen, L., Guo, J.H., 2010. Ca. 2.5 billion year old coeval ultramafic–mafic and syenitic dykes in Eastern Hebei: implications for cratonization of the North China Craton. Precambrian Research 180, 143–155.
Liu, S., 2004. The Mesozoic Magmatism and Crustal Extension in Shandong Province, China — Additional Discussing the Relationship between Lamprophyres and Gold Mineralization. (in Chinese) Ph.D. thesis Inst. of Geochem., Chin. Acad. of Sci., Guiyang (in Chinese).
Liu, S., Zou, H.B., Hu, R.Z., Zhao, J.H., Feng, C.X., 2006. Mesozoic mafic dikes from the Shandong Peninsula, North China Craton: petrogenesis and tectonic implications. Geochemical Journal 40, 181–195.
Liu, S., Hu, R.-Z., Gao, S., Feng, C.-X., Qi, L., Zhong, H., Xiao, T., Qi, Y.-Q., Wang, T., Coulson, I.M., 2008. Zircon U–Pb geochronology and major, trace elemental and Sr–Nd–Pb isotopic geochemistry of mafic dykes in western Shandong Province, east China: constrains on their petrogenesis and geodynamic significance. Chemical Geology 255, 329–345.
Liu, S., Hu, R., Gao, S., Feng, C., Qi, Y., Wang, T., Feng, G., Coulson, I.M., 2008. U–Pb zircon age, geochemical and Sr–Nd–Pb–Hf isotopic constraints on age and origin of alkaline intrusions and associated mafic dikes from Sulu orogenic belt, Eastern China. Lithos 106, 365–379.
Liu, S., Hu, R., Gao, S., Feng, C., Yu, B., Feng, G., Qi, Y., Wang, T., Coulson, I.M., 2009. Petrogenesis of Late Mesozoic mafic dykes in the Jiaodong Peninsula, eastern North China Craton and implications for the foundering of lower crust. Lithos 113, 621–639.
Liu, Y.S., Hu, Z.C., Zong, K.Q., Gao, C.G., Gao, S., Xu, J., Chen, H.H., 2010. Reappraisement and refinement of zircon U–Pb isotope and trace element analyses by LA-ICP-MS. Chinese Science Bulletin 55, 1535–1546.
Liu, S., Hu, R., Gao, S., Feng, C., Coulson, I.M., Feng, G., Qi, Y., Yang, Y., Yang, C., Tang, L., 2012. U–Pb zircon age, geochemical and Sr–Nd isotopic data as constraints on the petrogenesis and emplacement time of the Precambrian mafic dyke swarms in the North China Craton (NCC). Lithos 140–141, 38–52.
Liu, S., Hu, R., Gao, S., Feng, C., Feng, G., Qi, Y., Coulson, I.M., Yang, Y., Yang, C., Tang, L., 2012. Geochemical and isotopic constraints on the age and origin of mafic dikes

from eastern Shandong Province, eastern North China Craton. International Geology Review 54, 1389–1400.
Liu, S., Hu, R., Gao, S., Feng, C., Coulson, I.M., Feng, G., Qi, Y., Yang, Y., Yang, C., Tang, L., 2013. Zircon U–Pb age and Sr–Nd–Hf isotopic constraints on the age and origin of Triassic mafic dikes, Dalian area, Northeast China. International Geology Review 55, 249–262.
Ludwig, K.R., 2003. User's manual for Isoplot/Ex, Version 3.00. A Geochronological Toolkit for Microsoft Excel: Berkeley Geochronology Center Special Publication, 4 1–70.
Lugmair, G.W., Harti, K., 1978. Lunar initial $^{143}Nd/^{144}Nd$: differential evolution of the lunar crust and mantle. Earth and Planetary Science Letters 39, 349–357.
Meng, Q., Zhang, G., 1999. Timing of collision of the North and South China blocks: controversy and reconciliation. Geology 27, 123–126.
Middlemost, E.A.K., 1994. Naming materials in the magma/igneous rock system. Earth-Science Reviews 74, 193–227.
Peng, P., 2010. Reconstruction and interpretation of giant mafic dyke swarms: a case study of 1.78 Ga magmatism in the North China craton. Geological Society Special Publication, 338. Geological Society, London, pp. 163–178.
Peng, P., Zhai, M.-G., Zhang, H.-F., Guo, J.-H., 2005. Geochronological constraints on the Palaeoproterozoic evolution of the North China craton: SHRIMP zircon ages of different types of mafic dikes. International Geology Review 47, 492–508.
Peng, P., Zhai, M.G., Guo, J.H., Kusky, T., Zhao, T.P., 2007. Nature of mantle source contributions and crystal differentiation in the petrogenesis of the 1.78 Ga mafic dykes in the central North China craton. Gondwana Research 12, 29–46.
Peng, P., Zhai, M.-G., Li, Z., Wu, F.-Y., Hou, Q.-L., 2008. Neoproterozoic (~820 Ma) mafic dyke swarms in the North China craton: implication for a conjoint to the Rodinia supercontinent? Abstracts, 13th Gondwana Conference, Dali, China, pp. 160–161.
Peng, P., Guo, J.H., Zhai, M.G., Bleeker, W., 2010. Paleoproterozoic gabbronoritic and granitic magmatism in the northern margin of the North China craton: evidence of crust–mantle interaction. Precambrian Research 183, 635–659.
Peng, P., Bleeker, W., Ernst, R.E., Söderlund, U., McNicoll, V., 2011. U–Pb baddeleyite ages, distribution and geochemistry of 925 Ma mafic dykes and 900 Ma sills in the North China craton: evidence for a Neoproterozoic mantle plume. Lithos 127, 210–221.
Peng, P., Zhai, M.G., Li, Q.L., Wu, F.Y., Hou, Q.L., Li, Z., Li, T.S., Zhang, Y.B., 2011. Neoproterozoic (900 Ma) Sariwon sills in North Korea: geochronology, geochemistry and implications for the evolution of the south-eastern margin of the North China craton. Gondwana Research 20, 243–254.
Potts, P.J., Kane, J.S., 2005. International association of geoanalysts certificate of analysis: certified reference material OU-6 (Penrhyn slate). Geostandards and Geoanalytical Research 29, 233–236.
Rapp, R.P., Shimizu, N., Norman, M.D., 2003. Growth of early continental crust by partial melting of eclogite. Nature 425, 605–609.
Shaanxi Province Bureau of Geology and Mineral Resources, 1989. Regional Geology of Shaanxi Province (in Chinese with English abstract).
Steiger, R.H., Jäger, E., 1977. Subcommission on geochronology; convention on the use of decay constants in geochronology and cosmochronology. Earth and Planetary Science Letters 36, 359–362.
Sun, S.S., McDonough, W.F., 1989. Chemical and isotopic systematics of oceanic basalts: implications for mantle composition and processes. In: Saunders, A.D., Norry, M.J. (Eds.), Magmatism in the Ocean Basins: Geological Society Special Publication, London, pp. 313–345.
Tarney, J., Weaver, B.L., 1987. Geochemistry and petrogenesis of early Proterozoic dyke swarms. In: Halls, H.C., Fahrig, W.C. (Eds.), Mafic Dyke Swarms: Special Publication — Geological Association of Canada, Vol. 34, pp. 81–93.
Thompson, M., Potts, P.J., Kane, J.S., Wilson, S., 2000. An international proficiency test for analytical geochemistry laboratories — report on round 5 (August 1999). Geostandards and Geoanalytical Research 24, E1–E28.
Wang, Y.M., Gao, Y.S., Han, H.M., Wang, X.H., 2003. Practical Handbook of Reference Materials for Geoanalysis. Geological Publishing House (in Chinese).
Wu, F.Y., Yang, Y.H., Xie, L.W., Yang, J.H., Xu, P., 2006. Hf isotopic compositions of the standard zircons and baddeleyites used in U–Pb geochronology. Chemical Geology 234, 105–126.
Xu, J.W., Ma, G.F., Tong, W.X., Zhu, G., Lin, S.F., 1993. Displacement of Tancheng-Lujiang Wrench fault system and its geodynamic setting in the northwestern circum-Pacific. In: Xu, J. (Ed.), The Tanch eng-Lujiang Wrench system. John Wiley & Sons, pp. 51–74.
Yan, Y.X., 2005. Research on geochemistry and Sr, Nd and Pb isotope of the basic dyke swarms in Ziyang-Langao area, Shaanxi Province. Master's dissertation; Northwest University, China.
Yang, J.H., Chung, S.L., Zhai, M.G., Zhou, X.H., 2004. Geochemical and Sr–Nd–Pb isotopic compositions of mafic dikes from the Jiaodong Peninsula, China: evidence for vein-plus-peridotite melting in the lithospheric mantle. Lithos 73, 156–160.
Yuan, H.L., Gao, S., Liu, X.M., Li, H.M., Gunther, D., Wu, F.Y., 2004. Accurate U–Pb age and trace element determinations of zircon by laser ablation-inductively coupled plasma mass spectrometry. Geostandards Newsletter 28, 353–370.
Zhang, H.F., Sun, M., 2002. Geochemistry of Mesozoic basalts and mafic dikes, southeastern north China craton, and tectonic implications. International Geology Review 44, 370–382.
Zhang, X., 2010. The dynamic mechanism and Geological significance of mafic intrusion in the Ziyang-Zhenba area, south Qinling. Ph.D dissertation: Chang'an University, China.
Zhang, H.F., Sun, M., Zhou, X.H., Ying, J.F., 2005. Geochemical constraints on the origin of Mesozoic alkaline intrusive complexes from the North China Craton and tectonic implications. Lithos 81, 297–317.
Zhao, J.X., McCulloch, M.T., 1993. Melting of a subduction-modified continental lithospheric mantle: evidence from Late Proterozoic mafic dike swarms in central Australia. Geology 21, 463–466.
Zhao, G.C., Wilde, S.A., Cawood, P.A., Sun, M., 2001. Archean blocks and their boundaries in the North China Craton: lithological, geochemical, structural and P–T path constraints and tectonic evolution. Precambrian Research 107, 45–73.
Zhao, G.C., Wilde, S.A., Cawood, P.A., Sun, M., 2002. SHRIMP U–Pb zircon ages of the Fuping complex: implications for Late Archean to Paleoproterozoic accretion and assembly of the North China craton. American Journal of Science 302, 191–226.